Fundamental Analysis of Full-Duplex Gains in Wireless Networks

Shu Wang, Vignesh Venkateswaran, and Xinyu Zhang

***Abstract*— Full-duplex radio technology is becoming mature and holds potential to boost the spectrum efficiency of a point-to-point wireless link. However, a fundamental understanding is still lacking, with respect to its advantages over half-duplex in multi-cell wireless networks with contending links. In this paper, we establish a spatial stochastic framework to analyze the mean network throughput gain from full duplex, and pinpoint the key factors that determine the gain. Our framework extends classical stochastic geometry analysis with a new tool set, which allows us to model a tradeoff between the benefit from concurrent full-duplex transmissions and the loss of spatial reuse, particularly for CSMA-based transmitters with random backoff. We analytically derive closed-form expressions for the full-duplex gain as a function of link distance, interference range, network density, and carrier sensing schemes. It can be easily applied to guide the deployment choices in the early stage of network planning.**

***Index Terms*— Full duplex, capacity, stochastic geometry.**

I. Introduction

RECENT advances in radio hardware and signal processing are pushing full-duplex wireless communications close to commercialization [1]. However, existing work mostly focused on full-duplex PHY-layer implementation [2], [3] or MAC protocols [4], [5] that extend 802.11 CSMA/CA. Unlike half-duplex wireless networks whose asymptotics have been investigated extensively [6], the fundamental network-capacity implications of full-duplex remain largely underexplored.

In distributed wireless networks, contending nodes' transmissions need to be separated in *time, frequency,* and/or *space* to avoid excessive interference. Whereas full-duplex allows a pair of nodes to co-locate their transmissions in the same time slot and frequency band, their spatial interference footprint is heavier than a half-duplex pair. An accurate characterization of this trade-off can lead to a fundamental understanding of the full-duplex network capacity and the achievable gain, thus guiding the practical protocol design and network deployment.

Manuscript received January 8, 2016; revised July 31, 2016; accepted November 13, 2016; approved by IEEE/ACM TRANSACTIONS ON NETWORKING Editor A. Eryilmaz. This work was supported by the NSF under Grant CNS-1318292, Grant CNS-1343363, and Grant CNS-1350039.

S. Wang was with the Department of Electrical and Computer Engineering, University of Wisconsin-Madison, Madison, WI 53706 USA. He is now with The University of Chicago, Chicago, IL 60637 USA (e-mail: swang367@wisc.edu).

V. Venkateswaran was with the Department of Electrical and Computer Engineering, University of Wisconsin-Madison, Madison, WI 53706 USA. He is now with Cisco Systems Inc., San Jose, CA 95134 USA (e-mail: vvenkateswar@Wisc.edu).

X. Zhang is with the Department of Electrical and Computer Engineering, University of Wisconsin-Madison, Madison, WI 53706 USA (e-mail: xyzhang@ece.wisc.edu).

Digital Object Identifier 10.1109/TNET.2016.2633563

The objective of this work is to provide an analytical framework allowing one to access the key properties of full-duplex wireless networks running random access MAC protocols. The insights we seek include, *e.g.*, what is the expected network throughput (gain) when using full-duplex radios compared with half-duplex ones? What are the key factors that determine the gain and how to engineer such design knobs to maximize full-duplex's potential?

For such an analytical model, the main challenge lies in a need to take into account interference, random contention, and the resulting spatial reuse among contending links. Such factors, of course, are topology dependent. One cannot traverse the enormous number of possible configurations, but must instead consider a statistical spatial model for the node locations, and extracts insights from there.

Following this principle, we assume certain statistical distribution of AP/client locations, and derive spatial averages of critical network quantities, *e.g.*, interference and spatial density of successful transmitters. Such a spatial averaging technique, widely referred to as *stochastic geometry* [7], has been used in a variety of wireless network examples, like ad-hoc networks, in order to perform average-case analysis of network throughput, by modeling the interference experienced by nodes under a random access MAC protocol.

It is, however, non-trivial to apply the classical stochastic geometry model to full-duplex networks, because of two new barriers. *First*, existing stochastic geometry analysis [8], [9] uses a hard-core point process (HCPP) to model the distribution of winning transmitters. The contention region of a point in HCPP is defined by a unit disc containing no other points. With full-duplex, the spatial footprint of two neighboring transmitters can become correlated, which can no longer be handled by conventional stochastic geometry models. *Second*, existing models only focus on winning transmitters after CSMA/CA contention, but ignore the receiver which itself has an exclusive region and is vulnerable to artifacts of carrier sensing such as hidden terminals. Such artifacts are critical to spatial reuse and to the real gain from full-duplex.

In light of the above challenges, we propose a new stochastic framework that can analyze the average spatial footprint of a *typical* full-duplex pair, as well as the spatial distribution of full-duplex pairs that win contention. Our approach leads to closed-form expressions for the average throughput of full-duplex networks with Poisson-bipolar distributed links. It also gives closed-form analysis of half-duplex throughput under carrier sensing artifacts, *e.g.*, hidden/exposed terminals. Consequently, we can derive the full-duplex throughput gain under a variety of topological parameters and protocol imperfectness.

Our analysis starts with full-duplex ALOHA, the basic random access protocol where each node transmits with a fixed probability and without carrier sensing. Then, we extend the model to the more sophisticated CSMA. We find that the most critical factor that determines full-duplex gain is the mean link distance d relative to the carrier sensing range. A smaller d amplifies full-duplex gain since, intuitively, it reduces the interference footprint of a full-duplex link. For a fixed d, full-duplex gain tends to be larger in a very sparse deployment of APs, yet the gain saturates quickly as density increases. Surprisingly, we found that full-duplex ALOHA has even lower throughput than half-duplex ALOHA as n and d go beyond a certain level. The fundamental reason again lies in much heavier interference footprint.

More interestingly, we found a major contributing factor to full-duplex gain in CSMA networks lies in full-duplex nodes' capability to implicitly remove hidden/exposed terminals. Thus, the full-duplex gain tends to be amplified under imperfect carrier sensing.

The rest of this paper is structured as follows. We first present a background on stochastic geometry and our network models in Sec. II. Then we analyze the full-duplex gain under two sets of interference models, in Sec. III and IV. In each interference models, we will start with ALOHA, and then extend to CSMA-like wireless network. This is due to that, in ALOHA, each source independently transmit data whenever it has frames to be transmitted. However, for CSMA protocol, each source need to verifies the channel before any transmission. Sec. V discusses related work and finally, Sec. VI concludes the paper.

II. Background and Overview of Network Models

In this section, we present the essential models and assumptions underlying our analytical framework.

A. A Primer on Stochastic Geometry and Its Limitations

Stochastic geometry provides average-case analysis of network throughput, wherein the averages are made over a large number of nodes randomly located in the spatial domain.

Recent stochastic geometry models of 802.11 CSMA networks commonly apply a two-step approach [8]. *First*, nodes are assumed to be deployed following a Poisson Point Process (PPP). Then, the distribution of simultaneously active transmitters after CSMA contention is approximated by a Matèrn hard core point process (HCPP). Simply put, the HCPP *thins* the parent PPP and models the winning nodes after random backoff. *Second*, the interference experienced by a typical winning node is approximated by the interference resulting from a PPP which has the same intensity as the HCPP. Such approximation has been shown to be fairly accurate, mainly because the exact locations of the active transmitters matter less than the number of other active transmitters (interferers) and their relative distances. Given the approximated HCPP, network performance metrics such as transmission success probability (under interference) and throughput can be easily derived.

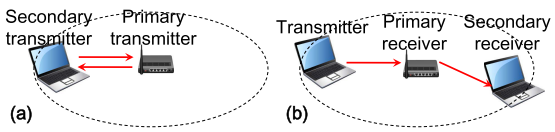

Fig. 1. Full-duplex transmission modes: (a) bidirectional transmission and (b) cut-through transmission. Ellipse indicates transmission range.

When applied to modeling the full-duplex gain, existing stochastic geometry models fall short of accuracy from three aspects. *(i)* They mainly focus on potential transmitters through a homogeneous point process model. The spatial reuse between transmitters and receivers cannot be modeled but is the most critical factor that determines the full-duplex gain [10]. *(ii)* They assume a unit disk exclusive region around each transmitter, and omit the carrier sensing artifacts, such as exposed and hidden terminals, which again account for the discrepancies in theoretical and practical limit of both half-duplex and full-duplex networks. *(iii)* They commonly approximate the received signal-to-interference-plus-noise ratio (SINR) using the SINR at the transmitter side, yet whether a transmission succeeds depends SINR at the receiver side (or both sides for full-duplex).

We remedy the above limitations by marrying stochastic geometry with the two interference models proposed in Gupta and Kumar's seminal work on ad-hoc network capacity analysis [6]. Below we provide more details of our model.

B. Full-Duplex Communication Model

A full-duplex node can simultaneously transmit and receive different packets. State-of-the-art full-duplex radio [3] can isolate the self-interference from transmitted signals to received ones, although perfect elimination is infeasible. Our analysis mainly focuses on the network-level impacts of full-duplex transmissions, assuming perfect full-duplex radio hardware.

When applied to multi-cell wireless LANs, full-duplex links can operate in two modes [2]. *Bidirectional transmission mode* (Fig. 1(a)) allows a pair of AP-client to transmit packets to each other simultaneously. *Cut-through transmission mode* (Fig. 1(b)) enables a full-duplex AP to simultaneously serve two clients, one for uplink and the other downlink. When applied to multi-hop networks, it is also referred to as wormhole relaying [10]. We first focus on the former mode, and then prove that the latter results in lower capacity (Sec. III-D.4). In what follows, all references to "full-duplex" means the bi-directional mode, unless noted otherwise.

C. Network Topology Model

We model the locations of transmitters/receivers as some realizations of random point process. Unlike existing CSMA stochastic geometry analysis that commonly focus on Poisson-distributed transmitters (Fig. 2(a)), we model the transmitter *and* receiver locations using a *Poisson bipolar model* [11].

For a *half-duplex network*, transmitters are distributed following a PPP. Each transmitter T_X associates with a receiver R_X, located in a direction θ (Fig. 2(b)), random uniformly distributed in $[0, 2\pi)$. We first assume link distance is fixed to d, and then generalize the model to random link distance

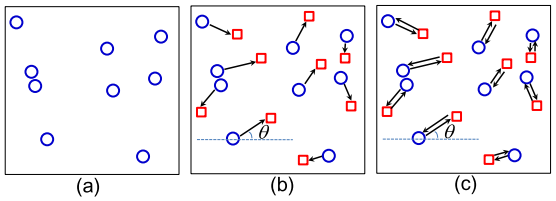

Fig. 2. (a) Existing stochastic model widely assumes Poisson distributed potential transmitter *nodes*. (b) Our half-duplex model focuses on *links* with Poisson bipolar model with mean link distance d. (c) Our full-duplex model focuses on bi-directional transmission *links*.

(Sec. III-D). The links in a *full-duplex network* follow the same distribution, except that a receiver is a transmitter at the same time (assuming bi-directional mode). For naming purpose, we refer to the node that initializes the full-duplex transmission as *primary transmitter* T_1 and the other as *secondary transmitter* T_2. The ordering does not affect our analysis.

Our model of a network with Tx/Rx pairs can be considered as a snapshot of a multi-cell WLAN with multiple clients per cell, wherein every AP is communicating with one associated client at any one time instant. Over time, the network can be considered as realization of multiple snapshots, and its performance mainly depends on the mean spatial throughput (density of successful transmissions) in each snapshot.

D. Contention and Interference Models

Our analysis focuses on two classical random-access contention protocols: ALOHA and CSMA.

1) ALOHA Networks: In ALOHA networks, every node can access the channel independently with a certain probability p_m without carrier sensing. Therefore, this mechanism might cause excessive collisions, and finally leads to low throughput. Compared with CSMA, ALOHA has higher collision rate and lower efficiency. However, the simplicity of ALOHA enables more tractable models, and it plays a fundamental role for other MAC protocol analysis.

2) CSMA-Based Networks: CSMA-based networks adopt a listen-before-talk strategy. If the channel is sensed to be busy, then the transmitter defers its transmission to avoid collision. Our analysis of CSMA networks inherits the simplicity of the interference models from Gupta and Kumar [6], which still hold true for full-duplex radios.

Protocol Model: In the protocol model, each transmitter has a fixed transmission range, interference range, and carrier sensing range. For simplicity, the interference and carrier sensing range are assumed to be the same value R_I, whereas the transmission range R_S can be smaller. A successful transmission depends on two conditions: *First*, the transmitter can be activated after carrier sensing and contention, *i.e.*, the transmitter has the lowest backoff counter among all candidates it can sense. Effectiveness of the carrier sensing depends on the sensing models, and will be treated case-by-case in Sec. III. *Second*, no other concurrent transmitters are activated within the corresponding receiver's interference range.

Physical Model: The physical model differs in the second condition. Instead of a fixed interference range, the transmission succeeds only if the link SINR exceeds a threshold β. The interference power is the cumulative interference from all concurrent transmitters, which still exist outside the transmitter's carrier sensing range after CSMA contention. We defer the formal mathematical definition to Sec. IV.

III. Full-Duplex Gain Under the Protocol Model

In this section, we describe our stochastic geometry framework that establishes a closed-form analysis of full-duplex gain under the protocol interference model. The analysis derives the spatial throughput of both ALOHA and CSMA-based full-duplex networks. Besides, in order to derive the expected throughput gain from full-duplex, our analysis needs to model carrier sensing artifacts of half-duplex networks, including the hidden/exposed terminals and use of RTS/CTS.

In each case, the analysis follows two major steps: *(i)* analyze the *mean contention region* around a *typical* pair of nodes. *(ii)* derive the probability of successful transmission for the typical pair that runs the CSMA random backoff, given the Poisson bipolar distributed contending links within its mean contention region. Then we compute and compare the full-duplex spatial throughput with all the half-duplex models to obtain the full-duplex gain in each case.

A. Mean Contention Region (MCR)

We first introduce a novel analytical technique called mean contention region (MCR) that overcomes the aforementioned limitations of classical stochastic geometry models.

Definition: Given a typical link $\mathcal{L}_o$ and a bounded region $\Omega \in \mathbb{R}^2$ around $\mathcal{L}_o$. We arbitrarily partition Ω into n small regions represented by their areas: $\Delta\Omega_1, \Delta\Omega_2, \cdots, \Delta\Omega_n$. Let $\sigma = \max_{1\le j\le n} \Delta\Omega_j$. We randomly select a point X_i from region $\Delta\Omega_i$, and define the *Mean Contention Region* as,

$$\lim_{\sigma\to 0} \sum_{i=1}^{n} p(X_i)\Delta\Omega_i, \tag{1}$$

where $p(X_i)$ is the probability that a transmitter of another link $\mathcal{L}_i$ located at X_i contends with typical link $\mathcal{L}_o$. If the limit exists and is unique, then we can cast it as: $\int_\Omega p(X)d\Omega$. Since $p(X)$ is a continuous function on a bounded region, the integral exists and is finite. □

Intuitively, MCR represents a spatial average of the area within which contenders/interferers may be located. Since the link locations follow a stationary distribution, it suffices to analyze the MCR of a *typical* link $\mathcal{L}_o$, comprised of a transmitter and a receiver (or two full-duplex bi-directional transmitters).

In half-duplex ALOHA networks, a transmission succeeds when *there is no other receiver within the transmitter's interference range, and no other transmitter within the receiver's interference range*. Essentially, this condition is the same as that in half-duplex CSMA with perfect carrier sensing. Therefore, these two types of networks share the same spatial reuse region, and hence the same MCR. Similarly, full-duplex ALOHA and CSMA networks have the same MCR. However, the eventual probability of a successful transmission differ due to the lack of carrier sensing in ALOHA. We defer the related MCR calculation in Sec. III-A.1 and Sec. III-A.4, and spatial distribution of successful transmissions in Sec. III-B.

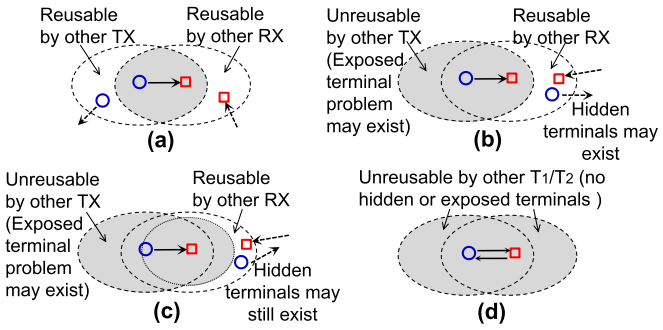

Fig. 3. Spatial reuse effects due to carrier sensing: (a) half-duplex networks with perfect carrier sensing; (b) half-duplex networks with imperfect carrier sensing; (c) RTS/CTS reduces hidden terminals but does not completely remove them; (d) full-duplex results in perfect carrier sensing. To simplify the illustration, we assume interference range and carrier sensing range overlap.

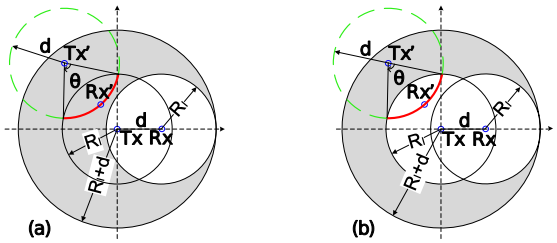

Fig. 4. Analyzing mean contention region of half duplex network with (a) perfect carrier sensing, and (b) imperfect carrier sensing.

For CSMA networks, the definition of contenders/ interferers, and the corresponding $p(X)$, depend on not only the duplex mode, but also the carrier sensing. Hence the MCR needs to be analyzed separately, for 4 different categories: half-duplex with perfect carrier sensing; half-duplex with imperfect carrier sensing; half-duplex with RTS/CTS signaling; and full-duplex.

1) Half-Duplex With Perfect Carrier Sensing: Perfect carrier sensing assumes perfect knowledge of contenders: each transmitter is well aware of which receivers it interferes with and which transmitters interfere with its receiver. Therefore, there exist no hidden/exposed terminals and spatial reuse is perfect (Fig.3(a)). This model is especially useful considering the recent advances in cross-layer implementation that minimizes the impact of hidden [12] and exposed terminals [13]. It is also the basic assumption behind Gupta and Kumar's protocol model for CSMA networks [6]. The following theorem offers a closed-form characterization of the corresponding MCR. For simplicity of exposition, we only provide the essential steps behind our analysis.

Theorem 1: The mean contention region for half-duplex CSMA networks with perfect carrier sensing is given by

$$V_{HP} = \pi R_I^2 + \frac{2}{\pi}\int_{R_I-d}^{R_I+d}(\pi-\theta)\theta r dr \tag{2}$$

$$\theta = \arccos\left(\frac{d^2+r^2-R_I^2}{2dr}\right). \tag{3}$$

Proof: Consider a typical link $\mathcal{L}_o$ whose transmitter T_X is located at the origin and its receiver at distance d along the x-axis (Fig. 4(a)).

First, the receiver's interference range (white area in Fig. 4(a)) should be counted deterministically within MCR (first term on the RHS of Eq. (2)), because any transmitter from other contenting link $\mathcal{L}'$ therein will contend with the typical link $\mathcal{L}_o$.

Second, consider a contending link $\mathcal{L}'$ whose transmitter $T_{X'}$ is within the shaded area in Fig. 4(a). If its receiver $R_{X'}$ is located within the interference range of T_X (red solid arc), then $R_{X'}$ will be interfered. Otherwise (green dashed arc), it needs not contend with the typical link and can transmit concurrently under perfect carrier sensing. Under Poisson bipolar model, the orientation of a receiver *w.r.t.* its transmitter is uniformly distributed in $[0, 2\pi)$. Thus, we can obtain the probability of $R_{X'}$ located in T_X's interference range by calculating the ratio of θ to 2π. Since this probability $p(X)$ depends on the transmitter's location, we can integrate the probability throughout the shaded area to obtain the spatial average (second term on the RHS of Eq. (2)).

For any other transmitter outside the above two regions, its receiver $R_{X'}$ can never fall within T_X's interference range, and thus it should not be counted into the MCR. □

2) Half-Duplex With Imperfect Carrier Sensing: In the basic 802.11 protocol (Fig. 3(b)), a node defers its transmission whenever it senses a busy channel. This mechanism reduces the risk of collision but often leads to the *exposed terminal* problem, *i.e.*, some nodes may not interfere a receiver, but are unnecessarily suppressed by the corresponding transmitter. In addition, it suffers from the *hidden terminal* problem, *i.e.*, other nodes outside the ongoing transmitter's carrier sensing range but inside the ongoing receiver's interference range can still cause collisions. We refer to this category of protocol as *imperfect carrier sensing*, and analyze the MCR as follows.

Theorem 2: Under imperfect carrier sensing, the mean contention region for CSMA networks is given by

$$V_{HI} = V_u + \frac{2}{\pi}\int_{R_I}^{R_I+d}(\pi-\theta)\theta r dr \tag{4}$$

$$V_u = 2\pi R_I^2 - 2R_I^2\arccos(\frac{d}{2R_I}) + d\sqrt{R_I^2-\frac{d^2}{4}} \tag{5}$$

$$\theta = \arccos\left(\frac{d^2+r^2-R_I^2}{2dr}\right) \tag{6}$$

Proof sketch: The transmitter T_X suppresses all other transmitters within its interference range which, together with the receiver's interference range, become a deterministic contention region (the V_u term above, corresponding to the white region in Fig. 4(b)). Spatial average of contention region for the shaded area can be derived in a similar way to Theorem 1. □

3) Half-Duplex With RTS/CTS Signaling: An enhanced version of 802.11 uses RTS/CTS to alleviate hidden terminals (Fig. 3(c)). Yet it still bears the exposed terminal problem. Moreover, there may still be hidden terminals outside the CTS transmission range but within the receiver's interference range. Denote the transmission range as R_S, then we can derive the MCR under RTS/CTS signaling as follows.

Theorem 3: The mean contention region for half duplex network using RTS/CTS is given by

$$V_{HRC} = \begin{cases} V_1 + V_2 + V_3 + 2(V_4 - V_5) & d > R_I - R_S \\ V_{HI} & d \le R_I - R_S \end{cases} \tag{7}$$

$$V_1 = 2\pi R_I^2 - 2R_I^2 \arccos(\frac{d}{2R_I}) + d\sqrt{R_I^2 - \frac{d^2}{4}} \tag{8}$$

$$V_2 = \frac{2}{\pi}\int_{R_I}^{R_I+d} (\pi - \gamma_1 - \theta_2)\theta_1 r dr \tag{9}$$

$$V_3 = \frac{2}{\pi}\int_{R_I}^{R_S+d} (\pi - \gamma_2 - \theta_3)\theta_4 r dr \tag{10}$$

$$V_4 = \frac{1}{2\pi}\int_0^d \int_{\theta_5-\gamma_2}^{\pi-\theta_6+\gamma_1} (\varphi_1 + \varphi_2 + \varphi_3) r dr d\theta \tag{11}$$

$$V_5 = \frac{1}{2\pi}\int_{R_S}^{R_I} \int_{\pi-\theta_1}^{\pi-\gamma_2-\theta_3} (\varphi_4 + \varphi_5 + \theta_4) r dr d\theta \tag{12}$$

The γ_1, γ_2, θ_1 to θ_5 and φ_1 to φ_5 are intermediate parameters, deferred to Appendix VI-A for simplicity of exposition.

We omit the proof because it is similar to the full-duplex case below, which is of more interest.

4) Full-Duplex: For full-duplex links, we assume a carrier sensing model similar to the FuMAC in [14]. A bi-directional full-duplex transmission can start only if both the primary and secondary transmitter sense an idle channel. Such synchronous full-duplex scheme has proven to have superior performance than one that mixes half-duplex with full-duplex transmissions [14]. In addition, *(i)* it eliminates hidden terminals because every receiver is a transmitter at the same time that uses its transmission as a busy-tone to protect itself from interferers. *(ii)* exposed terminals no longer exists, because no transmitter can coexist with other transmitter (and simultaneously a receiver) within the carrier sensing range anyway (Fig. 3(d)).

In other words, *full-duplex carrier sensing implicitly removes the hidden/exposed terminals*. Our later analysis will show this is where the main benefit of full-duplex comes from. Under this protocol, the MCR can be characterized as follows.

Theorem 4: The mean contention region for a typical full-duplex link is given by

$$V_F = V_1 + 2V_2 + 2V_3 \tag{13}$$

$$V_1 = 2\pi R_I^2 - 2R_I^2 \arccos(\frac{d}{2R_I}) + d\sqrt{R_I^2 - \frac{d^2}{4}} \tag{14}$$

$$V_2 = \frac{2}{\pi}\int_{R_I}^{R_I+d} (\pi - \theta_2 - \theta_3)\theta_1 r dr \tag{15}$$

$$V_3 = \int_0^d \int_{\frac{2\theta_4 + \theta_5 - \pi}{2}}^{\frac{3\pi - 2\theta_4 - \theta_5}{2}} (\frac{\varphi_1 + \varphi_2 + \varphi_3}{2\pi}) r dr d\theta \tag{16}$$

where θ_1 to θ_5 and φ_1 to φ_3 are intermediate parameters whose detaile expressions are available in Appendix VI-B.

Proof: The detailed proof is in Appendix VI-B. □

B. Spatial Density of Successful Transmissions

We now derive the mean transmission density, *i.e.*, average number of successful transmissions per unit area, after the typical pair of nodes *contend* with peers in the MCR. We start with ALOHA network analysis, which is based on Matèrn Type I process. Based on Matèrn Type I's result, we will extend our framework to CSMA network, which is based on Matèrn Type II process.

1) Spatial Density of ALOHA Networks: For ALOHA networks (Sec. II-D.1), the distribution of successful transmitters can be modeled as a Matèrn Type I process [11] that *thins* the original PPP distributed based on the medium access probability p_m. After the Matèrn thinning and independent medium access, the *Palm retaining probability* that a point x of the process is retained equals $e^{-\mu p_m V}$, where μ is the density of the original PPP [11] and V is the contention region as defined *a priori*.

(i) For half duplex ALOHA networks, each transmitter independently decides to access the medium with probability p_m. Therefore, the active transmitters' distribution still follows a PPP, but with density $p_m\lambda_p$ (recall that λ_p denotes the original deployment density of all nodes). The contention region for half duplex ALOHA is the same as V_{HP} in Theorem 1, since both the deterministic contention region of the receiver's interference ranges (white area in Fig. 4(a)) and probabilistic contention region of outside area (gray area in Fig. 4(a)) are the same as before. According to the *Palm retaining probability* mentioned above, the success probability of a typical half-duplex pair is thus given by: $\exp(-p_m\lambda_p V_{HP})$, and successful density is $\lambda_{HA} = p_m\lambda_p \exp(-p_m\lambda_p V_{HP})$.

(ii) For full-duplex, we assume the primary and secondary transmitters access the medium simultaneously, which can be realized using MAC protocols as in [14]. The contention region for full duplex ALOHA is the same as V_F in Theorem 4, since they have the same contention probability for the same location. Based on the *Palm retaining probability*, the success probability of a typical full-duplex pair is given by: $\exp(-p_m\lambda_p V_F)$, and successful density is $\lambda_{FA} = p_m\lambda_p \exp(-p_m\lambda_p V_F)$.

2) Spatial Density of CSMA Networks: The CSMA contention (Sec. II) can be modeled as a Matèrn Type II process [15] that *thins* the original PPP distributed contenders within the MCR. *Palm retaining probability* calculates the probability of that a point is retained within some locations ([16, Ch. 8]). Therefore, given a stationary independently marked PPP of intensity μ, a point x of the process having mark t is retained after Matèrn Type II thinning is given by $e^{-\mu t V}$, where V is the contention area. We adapt this result to our analysis and obtain the density of successful transmissions in the aforementioned 4 cases. Note that existing work widely uses a deterministic unit disk to model V, whereas our MCR model enables a spatial average analysis of the contention region that can model all 4 cases.

Half-Duplex CSMA Models: Let λ_p be the original deployment density of all potential transmitters. For the perfect carrier sensing case, the probability of the typical pair winning contention is $\exp(-\lambda_p t V_{HP})$, where V_{HP} follows Theorem 1. The mean successful density after contention can be obtain by

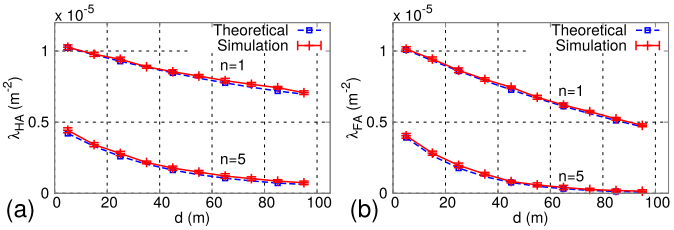

Fig. 5. Successful transmission density vs. link distance for (a) half-duplex ALOHA and (b) full-duplex ALOHA networks $R_I = R_C = 100, p_m = 0.6$.

averaging over all possible backoff counter t as:

$$\lambda_{HP} = \lambda_p \int_0^1 e^{-\lambda_p V_{HP} t} dt = \frac{1}{V_{HP}} \left(1 - e^{-\lambda_p V_{HP}}\right) \qquad (17)$$

Similarly, we can derive the successful transmission density for the imperfect carrier sensing case and RTS/CTS case as:

$$\lambda_{\rm HI} = \frac{1}{V_{\rm HI}} \left(1 - e^{-\lambda_p V_{\rm HI}}\right),$$

and

$$\lambda_{\rm HRC} = \frac{1}{V_{\rm HRC}} \left(1 - e^{-\lambda_p V_{\rm HRC}}\right)$$

One caveat should be noted about our MCR model for the half-duplex case with imperfect sensing and RTS/CTS. The model excludes other transmitters with smaller marks that lie in the elected receiver's interference region, but not those with larger marks, which may still cause collision to the receiver. However, our final analysis of $\lambda_{\rm HI}$ still gives an accurate approximation of the successful transmissions in the network. We provide simulation verification in Sec. III-B.3 and theoretical justification of our approximation in Sec. III-D.1.

Full Duplex CSMA Model:

For a full-duplex bi-directional link, we assume the primary and secondary transmitters hold the same backoff counter t, which can be realized using handshake protocols like [14]. Suppose t follows the same uniform distribution as in the half-duplex case, then the mean successful density of full-duplex transmissions is:

$$\lambda_F = V_F^{-1} (1 - e^{-\lambda_p V_F}). \qquad (18)$$

3) Simulation Verification: To verify the accuracy of the above closed-form models, we implement a simulator that simulates the carrier sensing, contention, and collision (due to hidden terminals) behaviors of each of the four network scenarios. The simulator runs in a round-based manner, and outputs the links that successfully transmit in each round. We run 20 randomly generated topologies with Poisson bipolar link distribution within a 100 km^2 region. Interference range R_I = 100m (equals carrier sensing range R_C) and link distance d ranges from 0 to R_I. We simulate a sparse network with per-node *neighbor density* of $n = 1$ and dense network with $n = 20$. The corresponding deployment density is $\lambda_p = n/(\pi R_I^2)$.

Fig. 5 and Fig. 6 compare the simulation results with the closed-form model. We see that our analytical results match closely with the simulated average across all the cases. In general, the successful transmission density decreases as d approaches R_I, because a longer link-distance is more vulnerable to interference and contention. This is true for both ALOHA and CSMA-based networks. In addition, note that the successful transmission density of the ALOHA networks drops much faster than that of CSMA-based networks when d increases, due to lack of carrier sensing or collision avoidance.

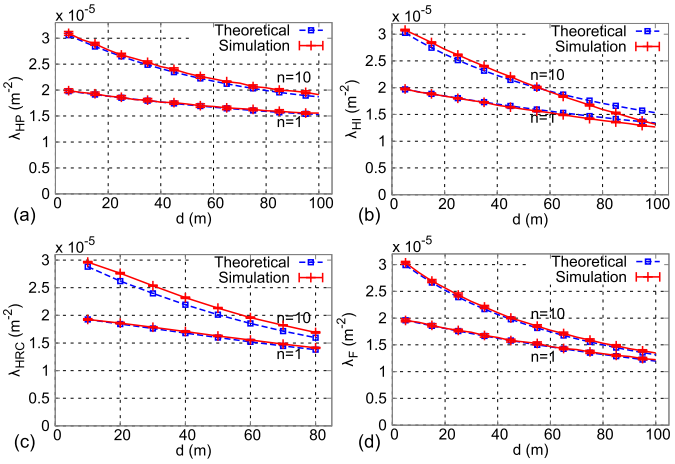

Fig. 6. Successful transmission density vs. link distance for half-duplex CSMA networks with: (a) perfect carrier sensing; (b) imperfect carrier sensing; (c) RTS/CTS; and (d) Full-duplex CSMA networks. $R_I = R_C = 100, R_S = 80$.

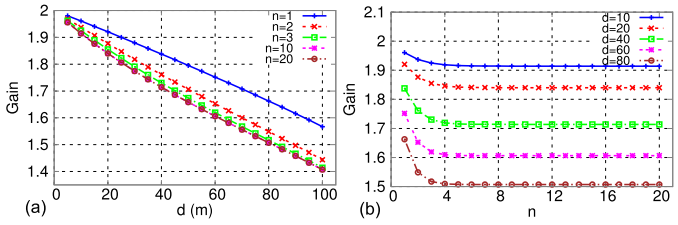

Fig. 7. Full-duplex gain over half-duplex network with perfect carrier sensing: (a) Gain diminishes as link distance approaches interference range (100 m), for all node density settings; (b) Gain diminishes and converges quickly as node density increases beyond a certain value.

For half-duplex networks, perfect carrier sensing results in higher density than the other two cases. RTS/CTS alleviates hidden-terminals, but the protection sacrifices spatial reuse, and results in similar density as the imperfect carrier sensing. Although the density of full-duplex pairs is similar to that of half-duplex when d is small, it decreases faster, implying that it is more vulnerable to loss of spatial reuse as d increases.

We proceed to analyze the impacts of the successful transmission density on full-duplex gain.

C. Throughput and Full-Duplex Gain

The mean density of successful transmissions can be regarded as spatial-average of the network throughput, which also equals its time-average across stationary topology realizations (Sec. II-C). Therefore, we can derive the full-duplex throughput gain over half-duplex perfect carrier sensing as: $G_{HP} = 2\lambda_F/\lambda_{HP}$, where a multiplier factor 2 is needed since each full-duplex pair supports double link transmission. The gain over other half-duplex cases in CSMA-based networks and ALOHA follows the same derivation.

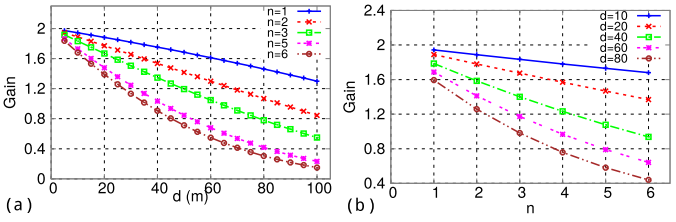

Fig. 8. (a) Gain of full-duplex over half-duplex ALOHA networks vs. link distance d for different n. Note n is related to node density as $n/\pi R_I^2 = \lambda_p$. (b) Gain of full-duplex over half-duplex ALOHA networks vs. n for different link distance d.

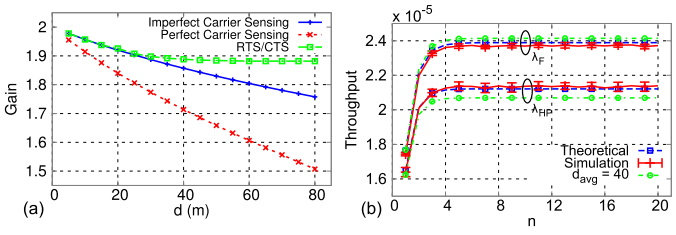

Fig. 9. (a). Gain under different carrier sensing schemes of half duplex network (b).Density of Successful Transmissions under $d \sim unif[0, 80]$ for Half-duplex networks with perfect carrier sensing and Full-duplex CSMA networks.

In Fig. 8, we show the full-duplex gain in ALOHA networks under the same simulation settings. It is clear that when link distance d increases to R_I, the gain drops quickly towards 0. In other words, *full-duplex ALOHA networks have even much lower mean throughput than the half-duplex counterparts, when mean link distance and node density go beyond a certain threshold.* The fundamental reason is that full-duplex networks have much heavier interference footprints than half-duplex networks, since both primary and secondary transmitters are occupying their own interference region and suppressing others. This becomes more significant when either link distance b or density n increases.

We plot the analytical full-duplex gain for all cases for CSMA-based network in Fig. 9, using similar parameters as above (Note that $R_I = R_C = 100$m). A common observation is that the gain may be close to 2 when d is near 0, but decreases as d approaches R_I. The reason behind is the same as the decreasing transmission density as discussed above. Fig. 7 also shows that the deployment density λ_p has minor impact under perfect carrier sensing: for a given d, the gain quickly saturates as λ_p increases. We found the imperfect sensing and RTS/CTS cases show similar behavior.

Among all cases (Fig. 9(a)), the gain drops fastest in the perfect carrier sensing case. The underlying reason can be understood from Fig. 3(a). For a half-duplex network with perfect carrier sensing, as d approaches R_I, a larger fraction of space can be reused by neighboring links, which diminishes the full-duplex's advantage in concurrent transmissions. The trend is consistent with the protocol model in [10]. On the other hand, the imperfect carrier sensing and RTS/CTS cannot fully take advantage of the spatial reuse, thus amplifying the full-duplex gain at larger d. We found that for the largest d ($d = R_I$) in the former two cases, the full-duplex gain is 1.4 and 1.71, and for the largest d ($d = R_S$) in the RTS/CTS case it is 1.88.

From the above analytical insights, we can conclude that *under the protocol interference model and CSMA contention model, the full-duplex gain is between 140% to 200%, and it largely comes from full-duplex's capability to overcome the imperfect carrier sensing in half-duplex.*

D. Discussion

1) Approximation of Hidden Terminal Scenario: Recall that our analysis of the imperfect half-duplex CSMA and RTS/CTS approximated the hidden terminal scenario. We hereby justify the approximation, starting with a simple 2-link case with imperfect carrier sensing. Consider two link pairs (T_{X1}, R_{X1}) and (T_{X2}, R_{X2}) with marks $t1$ and $t2$, respectively (Fig. 3(b)). Suppose T_{X2} lies in the interference region of R_{X1}. When $t1 < t2$, the pair (T_{X1}, R_{X1}) will be elected to transmit but (T_{X2}, R_{X2}) will not, because R_{X1} with lower mark lies in the interference region of T_{X2}. In reality, as T_{X1} and T_{X2} cannot hear each other, both pairs will transmit. However, (T_{X1}, R_{X1}) will fail due to T_{X2} interfering R_{X1}. In case when $t1 > t2$, (T_{X2}, R_{X2}) will be elected for transmission and will succeed. In both cases, we end up with one successful transmission, which is consistent with our analysis of V_{HI}.

Now we establish a theorem to show that it is sufficient to focus on the 2-link case, because the probability that more than one hidden terminals exist within the receiver's interference range is negligible.

Theorem 5: Under imperfect carrier sensing, the probability that more than one hidden terminal exists within the receiver's interference range can be bounded by,

$$\mathbb{P}(\mathbb{H}_{HI}) \leq 1 - \frac{2 - (2 + \lambda_p V_h) e^{-\lambda_p V_h}}{\lambda_p V_h e} \tag{19}$$

where V_h denotes the Rx's interference region excluding its Tx's interference region.

Proof: Hidden terminal happens when *(1)* T_X and R_X are in transmission period, and *(2)* another active $T_X{}'$ falls in R_X's interference range but outside T_X's, *i.e.*, $T_X{}' \in V_h$. So both T_X and $T_X{}'$ can be considered as retained after contention.

Let Φ be the original PPP, $\tilde{\Phi}$ the process after carrier sensing, and $\tilde{\Phi}(V)$ the number of points inside any region V after carrier sensing. Consider a typical Tx located at o, with interference region V_c. The event that o is retained is $\tilde{\Phi}(V_c) = 0$, *i.e.*, no other Tx falls within V_c. Similarly, more than one hidden terminal falls within V_h implies $\tilde{\Phi}(V_h) \geq 2$. Therefore, we can rewrite the probability as follows:

$$\begin{aligned}
\mathbb{P}(\mathbb{H}_{HI}) &= \mathbb{P}(\tilde{\Phi}(V_c) = 0 \cap \tilde{\Phi}(V_h) \geq 2) \\
&= \mathbb{P}(\tilde{\Phi}(V_h) \geq 2)\mathbb{P}(\tilde{\Phi}(V_c) = 0 | \tilde{\Phi}(V_h) \geq 2) && (20) \\
&\leq \mathbb{P}(\tilde{\Phi}(V_h) \geq 2) && (21) \\
&= 1 - \mathbb{P}(\tilde{\Phi}(V_h) = 0) - \mathbb{P}(\tilde{\Phi}(V_h) = 1) \\
&= 1 - \int_0^1 e^{-\lambda_p V_h t} dt - \int_0^1 \lambda_p V_h t e^{-\lambda_p V_h t} dt && (22) \\
&= 1 - \frac{2 - (2 + \lambda_p V_h) e^{-\lambda_p V_h}}{\lambda_p V_h} && (23)
\end{aligned}$$

Eq. (20) follows the conditional probability theorem. Eq. (22) is based on the hard core process [16, Ch. 3.5]. □

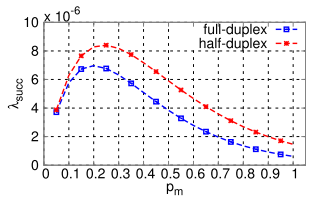

Fig. 10. Successful density for full- and half-duplex network under different medium access probability p_m (d = 50 and n = 3).

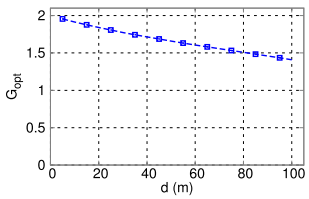

Fig. 11. Full-duplex gain over half-duplex ALOHA networks under optimal medium access probability p_m^*.

Our numerical calculation reveals that $\mathbb{P}(\mathbb{H}_{HI})$ increases slightly with node density, but is less than 4.7% even in highly dense networks with $n = 20$ per 100^2 m^2, and even when d is set to the maximum range of 100m. This implies that the two link case suffices to represent the impact of hidden terminals. The intuition behind such low probability $\mathbb{P}(\mathbb{H}_{HI})$ is that, if more than two potential transmitters fall within the small V_h region, very likely they can sense each other and at most one will become inactive after carrier sensing. For RTS/CTS, the same analysis and result holds, which we omit for brevity. Since V_h for RTS/CTS is less than that of imperfect carrier sensing, the corresponding probability for RTS/CTS is also less than that of imperfect sensing.

2) Optimal Medium Access Probability: In the ALOHA network, each transmitter access the medium with probability p_m, and it is interesting to see what is the optimal p_m value for both half-duplex and full-duplex network. In fig. 10, we plot the successful density under different medium access probabilities p_m. There are two observations: *(1)*, when p_m increases, the successful density first increase as well, after reaching the optimal points, it start to decrease. This can be understand, since, when p_m is relative small, it will cause less interference. However, when p_m is large enough, it cause huge interference due to uncoordinated transmission. *(2)*, the optimal successful density for half-duplex and full-duplex is achieved with different p_m value. Next, we will explore the optimal p_m from theoretical aspects.

Consider the successful density for half duplex is thus given by: $\lambda_{HA} = p_m\lambda_p \exp(-p_m\lambda_p V_{HP})$. To obtain the optimal p_m value, we need to calculate $\frac{\partial\lambda_{HA}}{\partial p_m} = 0$. By solving this equation, $p_{hf}^{opt} = 1/(\lambda_p V_{HP})$. Under this optimal p_{hf}^{opt}, the optimal successful density is $\lambda_{HA}^{opt} = 1/(eV_{HP})$. Similarly, for full duplex ALOHA network, the optimal medium access probability is $p_F^{opt} = 1/(\lambda_p V_F)$, and the optimal successful density for full-duplex is $\lambda_F^{opt} = 1/(eV_F)$.

From the theoretical derivation, we find optimal p_m depends on original point density λ_p as well as contention region. Also, if every transmitter use optimal p_m value, then the optimal successful density λ_{opt} only depends on contention region. Furthermore, the optimal gain of full-duplex over half-duplex equals $\lambda_{opt} = 2\lambda_{HA}^{opt}/\lambda_F^{opt} = 2V_F/V_{HP}$. We plot the optimal gain under different link distance in fig. 11, and when d increases, the optimal gain actually decreases.

3) Beyond Fixed Link Distance: All the analysis above has assumed the same fixed distance d for all links. We now show that the spatial average throughput is the same as that under a random uniformly distributed link distance with mean d.

Denote the link distance of the typical link as r_1 and a contending link as r_2. Unlike the previous MCR analysis, we should calculate the MCR *conditioned on* r_1 and r_2. Denote the corresponding MCR as $V(r_1, r_2)$. Suppose link distance is uniformly distributed from $[0, R_S]$, where R_S is the transmission range, we can obtain the density of successful transmission by averaging over all possible r_1 and r_2 as,

$$\frac{1}{R_S^2}\int_0^{R_S}\int_0^{R_S}\frac{1-e^{-\lambda_p V(r_1,r_2)}}{V(r_1,r_2)}dr_1dr_2 \qquad (24)$$

This applies to both the full-duplex and half-duplex cases. We now numerically compare the resulting transmission density with simulation, following similar setup as in the fixed-d case (Sec. III-B.3). Fig. 9(b) shows that the results from Eq. (24) are in close agreement with simulation. We only show perfect carrier sensing for half-duplex, without loss of generality. Given $R_S = 80$m (mean link distance $d = 40$m), we also our previous fixed distance model with that of the uniformly distributed case in Fig. 9(b) and we can see that the results match closely.

4) Full-Duplex Cut-Through Transmission Mode: Using some elements of the foregoing analysis, and by extending the Poisson Bipolar model, we now prove that the cut-through transmission is always inferior to the bi-directional transmission mode. Denote the transmitter T, primary receiver R_1 and secondary receiver R_2 (Fig. 1) using their locations X_i, Y_i and Z_i, respectively. We assume the X_i follows a PPP; Y_i is at distance d with a random orientation θ_i uniformly distributed in $[0, 2\pi)$. γ_i denotes the orientation of the secondary receiver *w.r.t.* the primary receiver. Since we need to ensure that Z_i is not interfered by X_i, the range of link distance d should be $[\frac{R_I}{2}, R_I]$ and the range of γ_i should be $[\theta - \arccos(\frac{R_I^2}{2d^2} - 1), \theta + \arccos(\frac{R_I^2}{2d^2} - 1)]$ in which it is uniformly distributed. Similar to the bi-directional full-duplex model we assume X_i and Y_i have the same back-off counter, which are uniformly distributed in $[0, 1)$. With this model setup, we can prove that:

Proposition 1: The network throughput under bi-directional transmission mode is no smaller than that of cut-through transmission mode with either perfect/imperfect carrier sensing.

Proof: From Fig. 3(d), the condition for successful bi-directional full-duplex transmission is that the shaded region cannot be reused by other T_1/T_2, and we can obtain MCR for it as V_F(Theorem 4). Based on Fig. 12 we elucidate the spatial occupation of cut-through transmission. Observing both the transmitter and secondary receiver operate in half-duplex mode. So we consider two situations here.

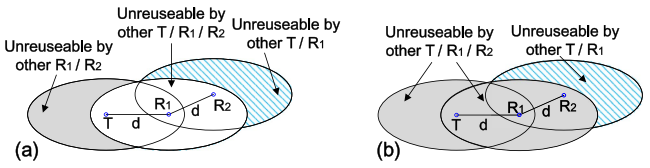

Fig. 12. Cut-through transmission with (a) Perfect carrier sensing (b) Imperfect carrier sensing.

First, considering the case of perfect carrier sensing, the condition for successful transmission as shown in Fig. 12(a) is the blue hatched region cannot be reused by any other T/R_1, grey shaded region cannot be reused by any other R_1/R_2 and the blank region cannot be reused any other $T/R_1/R_2$. If we assume that the blank region can be reused by other R_2 then the MCR of $R_1 \leftrightarrow R_2$ link is equivalent to that of a bi-directional link (V_F). In fact, if we restrict other R_2 from being present in the blank region, then the above MCR would be larger than V_F. Furthermore, as MCR for the grey region is nonzero, the total MCR for cut-through transmission with perfect carrier sensing is larger than that of a bi-directional link.

Second, for imperfect carrier sensing case, the successful transmission condition should be no other $T/R_1/R_2$ in the grey region and no other T/R_1 in the blue hatched region. Suppose that the grey region can be reused by other R_2. Then, the MCR of $T \leftrightarrow R_1$ link is equivalent to that of a bi-directional link. Actually, if allow other R_2 in the grey region then the above MCR would be larger than V_F. Furthermore, as the MCR for blue hatched region is nonzero, the total MCR for cut-through transmission with imperfect carrier sensing is larger than that of a bi-directional link as well.

We conclude that in either case the spatial occupation for cut-through transmission is always larger than that of bi-directional transmission, and therefore its network throughput is lower. □

IV. Full-Duplex Gain Under the Physical Model

In this section, we will consider full duplex gain under physical model for both ALOHA and CSMA contention. First, we will give the successful transmission probability of a half-duplex link under ALOHA contention based on previous research, and then obtain a lower bound on the successful transmission probability of a half-duplex link under CSMA contention, which is shown to be tight through simulation. We only focus on the imperfect carrier sensing (basic 802.11) case. Extension to other half-duplex cases is trivial and omitted. For the full duplex link, we obtain an upper-bound of links' successful transmission probability under ALOHA networks, and then derive an approximation of the full-duplex links' successful transmission probability. Subsequently, we calculate the full-duplex network throughput gain under each condition. Our analysis is built on the *Campbell's* theorem [17], *second-order product density* of a stationary point process and *Jensen's* inequality.

A. Modeling Transmission Success for Half-Duplex

Usually, the nearby interference is much higher than the noise power [7]. Therefore, for a typical link, the successful transmission probability equals the probability that its signal-to-interference ratio (SIR) exceeds a threshold β, conditioned on this link wins the CSMA or ALOHA contention.

1) Modeling Contention and SIR: For ALOHA contention, the winning transmitters can be modeled using Matèrn Type I point process. Assuming that every transmitter accesses the channel with an independent medium access probability p_m, and λ_p is the intensity of original PPP $\tilde{\Phi}_o$, then the winning transmitters in ALOHA networks should be a PPP Φ_m^H with density $p_m\lambda_p$.

We also leverage the Matèrn Type II point process [18] to model the winning transmitters in half-duplex CSMA contention. A transmitter of the original deployed PPP $\tilde{\Phi}_o$ is chosen for the Matèrn process if it has the least backoff counter among all other points that lie in its carrier sensing range R_C. Denote Φ_m^H as the thinned point process after all winning transmitters are chosen, then its intensity is [19]:

$$\lambda_m^h = \frac{1 - e^{-\lambda_p \pi R_C^2}}{\pi R_C^2} \tag{25}$$

where λ_p is the intensity of $\tilde{\Phi}_o$, *i.e.*, the deployment density.

In both situations, for a winning transmitter X_i, the receiver Y_i can successfully decode its packets only if its SIR satisfies:

$$SIR_{Y_i} := \frac{P h_{X_i Y_i} d^{-\alpha}}{\sum_{X_j \in \Phi_m^H, j \neq i} P h_{X_j Y_i} \|X_j - Y_i\|^{-\alpha}} > \beta \tag{26}$$

where P represents the transmission power and h_{XY} represents the channel fading coefficient from a transmitter X to a receiver Y. We assume the *Rayleigh* fading model, in which the $\{h_{XY}\}$ are a set of *i.i.d.* exponentially distributed random variables with mean $\mathbb{E}(h_{XY}) = 1$. The *path loss* from a node x to a node y is given by $\|x - y\|^{-\alpha}$, where $\|x - y\|$ is the *Euclidean* distance between the nodes and α is the path loss exponent.

2) Successful Transmission Probability: For ALOHA contention, the intensity of successful transmitters has been already established in previous work [20]. For completeness, we restate the result [20]:

Theorem 6: Under the physical model with ALOHA contention, the successful transmission probability is given by:

$$\mathbb{P}_{\Phi_m^H}(SIR_{Y_o} > \beta) = exp\left(-\lambda_p p_m d^2 \beta^{\frac{2}{\alpha}} C(\alpha)\right), \tag{27}$$

where $C(\alpha) = \frac{2\pi^2}{\alpha \sin(\frac{2\pi}{\alpha})}$.

For CSMA contention model, we consider a *typical* transmitter $X_o \in \Phi_m^H$, located at the origin o, and receiver Y_o at a distance d with orientation ϕ uniformly distributed in $[0, 2\pi)$. Then we calculate the probability in Eq. (26) under the *Reduced Palm distribution* $\mathbb{P}^{!o}_{\Phi_m^H}$ of Φ_m^H, since *Reduced Palm distribution* is used when we does not want to consider a point that a point process conditioned on ([16, Ch. 8.4]. $\mathbb{P}^{!o}_{\Phi_m^H}(SIR_{Y_o} > \beta)$ denotes the probability that the SIR at receiver is greater than β given that $X_o \in \Phi_m^H$, but not counting X_o's transmission as interference. With this setup, we can have:

Theorem 7: Under the physical model with CSMA contention, the successful transmission probability for a typical

Poisson bipolar distributed half-duplex link can be bounded as:

$$\mathbb{P}^{!o}_{\Phi^H_m}(SIR_{Y_o} > \beta) > \frac{1}{2\pi}\int_0^{2\pi} exp\left\{-\frac{\lambda_p^2}{\lambda_m^h}\int_0^{\infty}\int_0^{2\pi} k(r,\theta)\Delta(r,\theta,\phi)r\mathrm{d}r\mathrm{d}\theta\right\}\mathrm{d}\phi.$$

where $k(r,\theta)$ denotes the probability that two transmitters of $\tilde{\Phi}_o$ separated by a distance r and having a phase angle difference θ are retained in Φ^H_m and is given in [19]. $V(r)$ is the union of areas covered by the carrier sensing ranges of the two transmitters separated by a distance r and is given by $V(r) = 2\pi {R_C}^2 - 2{R_C}^2 \arccos(\frac{r}{2R_C}) + r\sqrt{{R_C}^2 - \frac{r^2}{4}}, 0 \le r \le 2R_C$ and, $\Delta(r,\theta,\phi) = \ln\left(1+\beta\left(\frac{d^2}{r^2+d^2-2dv\cos(\theta-\phi)}\right)^{\frac{\alpha}{2}}\right)$.

Proof: We first calculate the probability of SIR coverage at the receiver conditioned on its orientation ϕ with the horizontal, *i.e.*, we calculate $\mathbb{P}^{!o}_{\Phi^H_m}(SIR_{Y_o} > \beta \mid \phi)$. Then, in the end we get $\mathbb{P}^{!o}_{\Phi^H_m}(SIR_{Y_o} > \beta)$ by deconditioning on ϕ. To reduce notational complexity, in this proof we will henceforth refer to probability of coverage conditioned on ϕ as $\mathbb{P}^{!o,\phi}_{\Phi^H_m}(SIR_{Y_o} > \beta)$.

$$\mathbb{P}^{!o,\phi}_{\Phi^H_m}(SIR_{Y_o} > \beta) = \mathbb{P}^{!o,\phi}_{\Phi^H_m}\left(\frac{Ph_{X_oY_o}d^{-\alpha}}{\sum_{X_j\in\Phi^H_m} Ph_{X_jY_o}\|X_j - Y_o\|^{-\alpha}} > \beta\right)$$

$$= \mathbb{E}^{!o,\phi}_{\Phi^H_m, h_{X_jY_o}}\left[exp\left\{-\beta d^{\alpha}\sum_{X_j\in\Phi^H_m} h_{X_jY_o}\|X_j - Y_o\|^{-\alpha}\right\}\right] \quad (28)$$

$$= \mathbb{E}^{!o,\phi}_{\Phi^H_m}\left[\prod_{X_j\in\Phi^H_m}\mathbb{E}_{h_{X_jY_o}}\left[exp\left\{-\beta d^{\alpha}h_{X_jY_o}\|X_j - Y_o\|^{-\alpha}\right\}\right]\right] \quad (29)$$

$$= \mathbb{E}^{!o,\phi}_{\Phi^H_m}\left[exp\left\{-\sum_{X_j\in\Phi^H_m}\ln\left(1+\beta\left(\frac{d}{\|X_j - Y_o\|}\right)^{\alpha}\right)\right\}\right]$$

$$> exp\left\{-\mathbb{E}^{!o,\phi}_{\Phi^H_m}\left[\sum_{X_j\in\Phi^H_m}\ln\left(1+\beta\left(\frac{d}{\|X_j - Y_o\|}\right)^{\alpha}\right)\right]\right\} \quad (30)$$

$$= exp\left\{-\mathbb{E}^{!o,\phi}_{\Phi^H_m}\left[\sum_{(r,\theta)\in\Phi^H_m}\Delta(r,\theta,\phi)\right]\right\}$$

$$= exp\left\{-\frac{1}{\lambda_m^h}\int_0^{\infty}\int_0^{2\pi}\rho^{(2)}(r,\theta)\Delta(r,\theta,\phi)r\mathrm{d}r\mathrm{d}\theta\right\} \quad (31)$$

$$= exp\left\{-\frac{\lambda_p^2}{\lambda_m^h}\int_0^{\infty}\int_0^{2\pi} k(r,\theta)\Delta(r,\theta,\phi)r\mathrm{d}r\mathrm{d}\theta\right\} \quad (32)$$

To obtain Eq. (28), we condition on the point process Φ^H_m and $h_{X_jY_o}$ and use the fact that $h_{X_oY_o}$ is an exponential random variable with $\mathbb{E}(h_{X_oY_o}) = 1$. As $\{h_{X_jY_o}\}$ are a set of *i.i.d* random variables, we get Eq. (29). To get Eq. (30), we apply *Jensen's* inequality using the fact that $exp(-.)$ is a strictly convex function. We get Eq. (31) by applying *Campbell's* theorem [17] to the previous step. To get Eq. (32), we use the relation between *second-order product density* of the stationary point process Φ^H_m and $k(r,\theta)$ based on [21]. Finally, by deconditioning Eq. (32) *w.r.t* ϕ, we obtain Theorem 7. □

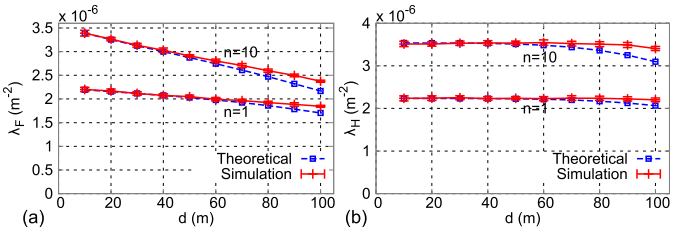

Fig. 13. Density of Successful Transmissions vs. link distance of (a) Half-duplex CSMA networks (b) Full-duplex CSMA networks under physical model.

Fig. 13(a) compares the lower-bound with our simulation results across 20 topologies. We observe that the bound matches tightly with the simulated mean successful transmission density, across the entire range of $0 < d \le R_S$ and for different λ_p (recall $\lambda_p = n/(\pi R_C^2)$).

B. Modeling Transmission Success for Full-Duplex

In the case of full-duplex networks, a pair of nodes X_i and Y_i that are selected for transmission can successfully exchange packets between its nodes only if $SIR_{X_i} > \beta$ and $SIR_{Y_i} > \beta$, where SIR_{X_i} is the SIR considered at the primary transmitter X_i for its reception from the secondary transmitter Y_i, and SIR_{X_i}, as shown at the bottom of this page.

The SIR at the secondary transmitter Y_i can be defined similarly. The channel fading coefficients follow the same model as in the half-duplex case. Note however that the interference term is attributed to not only other primary transmitters X_j, but also the associated secondary transmitters Y_j.

Consider a given full-duplex pair q_i. Assuming a symmetric channel between the primary and secondary transmitter, we have $h_{X_iY_i} = h_{Y_iX_i} = h_i$. Also, as the magnitude of received signal power at a node is dominated by *path-loss*, we assume that the channel fading coefficients between different nodes of two pairs q_i and q_j are the same i.e. $h_{X_jX_i} = h_{X_jY_i} = h_{Y_jX_i} = h_{Y_jY_i}$. We denote the representative channel fading coefficient from pair q_j to pair q_i by h^i_j. So, we are left with one set of *i.i.d* representative channel fading coefficients $\{h^i_j\}$ between different pairs i and j. A successful transmission thus needs to satisfy the following conditions for SIR_{X_i} and SIR_{Y_i}:

$$SIR_{X_i} := \frac{h_i d^{-\alpha}}{\sum_{q_j\in\Phi^F_m, j\neq i} h^i_j\left(\|X_j - X_i\|^{-\alpha} + \|Y_j - X_i\|^{-\alpha}\right)} > \beta$$

$$SIR_{Y_i} := \frac{h_i d^{-\alpha}}{\sum_{q_j\in\Phi^F_m, j\neq i} h^i_j\left(\|X_j - Y_i\|^{-\alpha} + \|Y_j - Y_i\|^{-\alpha}\right)} > \beta$$

$$SIR_{X_i} := \frac{Ph_{Y_iX_i}d^{-\alpha}}{\sum_{(X_j,Y_j)\in\Phi^F_m, j\neq i} Ph_{X_jX_i}\|X_j - X_i\|^{-\alpha} + Ph_{Y_jX_i}\|Y_j - X_i\|^{-\alpha}} > \beta$$

As the process Φ_m^F is a Poisson point process, according to *Slivnyak's* Theorem [22], we can add a reference primary transmitter, say X_o, to the process with its secondary transmitter, say Y_o, at the origin. The probability that two nodes in a typical full-duplex pair (X_o, Y_o) successfully transmit to each other is then given by $\mathbb{P}^{!o}_{\Phi_m^F}(SIR_{X_o} > \beta, SIR_{Y_o} > \beta)$, which we derive as follows.

1) ALOHA Networks: In the case of full-duplex networks under ALOHA contention, we consider that every pair contends for channel access with a medium access probability p_m independent of the other pairs. That is, if a pair wins channel contention, both the nodes in the pair transmit synchronously to each other. Similarly, the winning transmitters should be a PPP Φ_m^F with density $p_m\lambda_p$, if the primary transmitters are distributed as homogeneous PPP with density λ_p.

Theorem 8: Under the physical model with ALOHA contention, the successful transmission probability for a typical full-duplex bi-directional link can be bounded by:

$$\mathbb{P}_{\Phi_m^F}(SIR_{X_o} > \beta,\, SIR_{Y_o} > \beta) \leq exp\left\{-2\pi p_m\lambda_p \int_0^\infty \frac{r}{1+(\beta d^\alpha)^{-1}\left(r^{-\alpha}+(r+d)^{-\alpha}\right)^{-1}}\,\mathrm{d}r\right\}$$

Proof: The probability that two nodes in a pair successfully transmit to each other can be upper bounded as,

$$\mathbb{P}_{\Phi_m^F}(SIR_{X_o} > \beta,\, SIR_{Y_o} > \beta) \;\leq\; \mathbb{P}_{\Phi_m^F}(SIR_{Y_o} > \beta). \tag{33}$$

We note here that we could have upper bounded the probability that two nodes in a pair successfully transmit to each other by $\mathbb{P}_{\Phi_m^F}(SIR_{X_o} > \beta)$ equivalently. As we consider a symmetric channel between X_o and Y_o, and the quantities $\mathbb{P}_{\Phi_m^F}(SIR_{X_o} > \beta)$ and $\mathbb{P}_{\Phi_m^F}(SIR_{Y_o} > \beta)$ are *spatial averages* this would not make a difference. Making similar assumptions about the channel fading coefficients as in the analysis of full-duplex CSMA networks, we have,

$$\begin{aligned}
&\mathbb{P}_{\Phi_m^F}(SIR_{Y_o} > \beta)\\
&= \mathbb{P}_{\Phi_m^F}\left(\frac{h_o d^{-\alpha}}{\sum_{q_j\in\Phi_m^F} h_j^o\left(\|X_j-Y_o\|^{-\alpha}+\|Y_j-Y_o\|^{-\alpha}\right)} > \beta\right)\\
&= \mathbb{P}_{\Phi_m^F}\left(h_o > \beta d^\alpha \sum_{q_j\in\Phi_m^F} h_j^o\left(\|X_j\|^{-\alpha}+\|Y_j\|^{-\alpha}\right)\right) \qquad (34)\\
&= \mathbb{E}_{\Phi_m^F,h_j^o}\left[exp\left\{-\beta d^\alpha \sum_{q_j\in\Phi_m^F} h_j^o\left(\|X_j\|^{-\alpha}+\|Y_j\|^{-\alpha}\right)\right\}\right] \qquad (35)\\
&\leq \mathbb{E}_{\Phi_m^F,h_j^o}\left[exp\left\{-\beta d^\alpha \sum_{X_j\in\Phi_m^F} h_j^o \left(\|X_j\|^{-\alpha}+(\|X_j\|+d)^{-\alpha}\right)\right\}\right]\\
&= \mathbb{E}_{\Phi_m^F}\left[\mathbb{E}_{h_j^o}\left[\prod_{X_j\in\Phi_m^F} exp\left\{-\beta d^\alpha h_j^o \left(\|X_j\|^{-\alpha}+(\|X_j\|+d)^{-\alpha}\right)\right\}\right]\right] \qquad (36)\\
&= \mathbb{E}_{\Phi_m^F}\left[\prod_{X_j\in\Phi_m^F} \mathbb{E}_{h_j^o}\left[exp\left\{-\beta d^\alpha h_j^o \left(\|X_j\|^{-\alpha}+(\|X_j\|+d)^{-\alpha}\right)\right\}\right]\right] \qquad (37)\\
&= \mathbb{E}_{\Phi_m^F}\left[\prod_{X_j\in\Phi_m^F} \frac{1}{1+\beta d^\alpha\left(\|X_j\|^{-\alpha}+(\|X_j\|+d)^{-\alpha}\right)}\right]\\
&= exp\left\{-p_m\lambda_p\int_{\mathbb{R}^2} 1 - \frac{1}{1+\beta d^\alpha\left(\|X_j\|^{-\alpha}+(\|X_j\|+d)^{-\alpha}\right)}\mathrm{d}X_j\right\} \qquad (38)\\
&= exp\left\{-2\pi p_m\lambda_p\int_0^\infty \frac{r}{1+(\beta d^\alpha)^{-1}\left(r^{-\alpha}+(r+d)^{-\alpha}\right)^{-1}}\mathrm{d}r\right\} \qquad (39)
\end{aligned}$$

We get Eq. (34) by replacing Y_o with 0 as Y_o is located at the origin. To get Eq. (35) we use the fact that h_o is an exponentially distributed random variable with $\mathbb{E}(h_o) = 1$. By replacing $\|Y_j\|^{-\alpha}$ in Eq. (36) with $(\|X_j\|+d)^{-\alpha}$ in Eq. (37), we get a lower bound on the total interference at the origin (which is the sum in Eq. (36)), which gives the upper bound in Eq. (37). We obtain Eq. (38) using the fact the $\{h_j^o\}$ is a set of *i.i.d* random variables. We obtain Eq. (39) using the probability generating functional of the Poisson point process Φ_m^F [23]. Finally, by combining Eq. (39) with (33) we get the statement of Theorem 8. ∎

2) CSMA-Based Networks: Similarly, we derive the successful transmission probability for full duplex bi-directional link under CSMA contention as follows.

Theorem 9: Under the physical model with CSMA contention, the successful transmission probability for a typical full-duplex bi-directional link can be approximated by:

$$\begin{aligned}
&\mathbb{P}^{!o}_{\Phi_m^F}(SIR_{X_o} > \beta,\, SIR_{Y_o} > \beta)\\
&\quad\approx \frac{1}{2\pi}\int_0^{2\pi} exp\left\{-\frac{\lambda_p^2}{2\pi\lambda_m^f}\int_0^\infty\int_0^{2\pi}\int_0^{2\pi} k(r,\theta,\phi,\delta)\,\Delta(r,\theta,\phi,\delta)r\mathrm{d}r\mathrm{d}\theta\mathrm{d}\delta\right\}\mathrm{d}\phi
\end{aligned}$$

where, $k(r,\theta,\phi,\delta)$ denotes the probability that two pairs q_i and q_j of $\tilde{\Phi}_o$ are retained in Φ_m^F and is given by,

$$k(r,\theta,\phi,\delta) = \begin{cases} 0, & (r,\theta,\phi,\delta) \in B_1\cup B_2\cup B_3\cup B_4\\ 2g(V_1), & \text{otherwise}\end{cases}$$

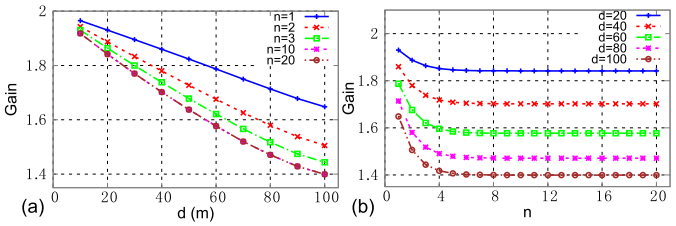

Fig. 14. Full-duplex gain under the physical model under CSMA contention: (a) Impact of link distance, under different node densities; (b) Impact of node density, under different link distance settings.

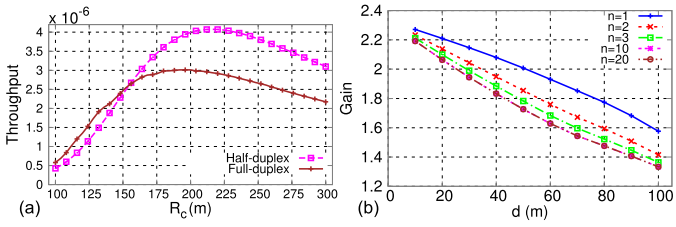

Fig. 15. (a) Spatial throughput vs. carrier sensing range. Optimal $R_C = 200m$ for full-duplex and $R_C = 216m$ for half-duplex (b) Gain of full-duplex over half-duplex CSMA networks under physical model using the optimal R_C.

and,

$$g(V_1) = \frac{V_1(1-e^{-\lambda_p V_F}) - V_F(1-e^{-\lambda_p V_1})}{\lambda_p^2 V_F V_1 (V_1 - V_F)}$$

where V_F follows Theorem 4, and λ_m^f equals λ_F (Eq. 18). V_1, B_1 to B_4 and $\Delta(r,\theta,\phi,\delta)$ are parameters detailed in .

Proof: Available in the technical report VI-C. □

In Fig. 13 (b) we compare the simulation results for the density of successful transmissions of full-duplex CSMA networks and the above approximation. We simulate 20 topologies and observe that the estimation obtained is in close agreement with the simulation results across different d and λ_p settings.

C. Full-Duplex Gain Under Physical Model

Under the physical model, the spatial network throughput can be calculated as the product of the intensity of concurrent transmissions and the probability that a transmission is successful. Here, we only focus only networks gain under CSMA contentions, since the full duplex gain under ALOHA contention can be derived in a similar way. The throughput for the half-duplex CSMA networks, denoted as T_H, is thus given by,

$$T_H = \lambda_m^h \, \mathbb{P}^{!o}_{\Phi_m^H}(SIR_{Y_o} > \beta)$$

where λ_m^h is given by Eq. (25) and $\mathbb{P}^{!o}_{\Phi_m^H}(SIR_{Y_o} > \beta)$ can be obtained from the result in Theorem 7.

For the full-duplex CSMA networks, the network throughput can be derived as,

$$T_F = 2\lambda_m^f \, \mathbb{P}^{!o}_{\Phi_m^F}(SIR_{X_o} > \beta,\ SIR_{Y_o} > \beta)$$

where λ_m^f is given by Eq. (18) and $\mathbb{P}^{!o}_{\Phi_m^F}(SIR_{X_o} > \beta,\ SIR_{Y_o} > \beta)$ can be obtained following Theorem 9. There is multiplication by a factor 2 because λ_m^f is the density of transmission pairs and every pair has two active transmissions.

In Fig. 14 we plot the network throughput gain of full-duplex over half-duplex CSMA networks, T_F/T_H, with varying link distance d and deployment density λ_p where $\lambda_p = n/\pi R_C^2$. *We observe that the full-duplex gain shows similar trend as in the protocol model*, *i.e.*, it approaches 2 as d is near 0, but decreases to around 1.4 as d approaches R_S.

We also observed that the carrier sensing range R_C is a crucial parameter that affects the spatial throughput. Fig. 15(a) plots the numerical spatial throughput under different R_C settings, with SIR threshold $\beta = 10$ dB, $\alpha = 4$ and maximum link distance 100m. A smaller R_C may not be able to protect the receiver from interference, whereas a larger R_C degrades spatial reuse between links. Remarkably, *the throughput-optimal R_C for full-duplex is smaller than that of half-duplex*, again because of full-duplex's capability of perfect carrier sensing. Each full-duplex receiver itself is a transmitter, and hence it does not require the other transmitter to extend R_C to protect it. From Fig. 15 (b) we can see that under the optimal R_C values the full-duplex can provide a throughput gain larger than 2 for smaller link distances (*e.g.*, 2.3× for $d = 10$m). This is another aspect that network planners need to consider to capitalize on full-duplex technology. Given the consistency of physical and protocol model, we expect a varying R_C will affect the full-duplex gain in the protocol model as well. We leave the detailed exploration for future work.

V. Related Work

Recent research on full-duplex mainly focuses on implementing new radio hardware architecture and signal processing algorithms. Choi *et al.* [2] is the first to realize single-channel full-duplex over ZigBee radios, which inspired substantial follow-on efforts. In particular, Bharadia *et al.* [3] recently implemented the first in-band full-duplex WiFi radio with a single antenna.

The development of full-duplex radios is marching steadily towards commercialization [1]. In contrast, the impact of full-duplex on higher network layers remains largely under-explored. Centralized scheduling and decentralized random access protocols [4], [5] have been proposed for full-duplex wireless LANs. Each of these protocols modifies the current CSMA MAC to capitalize on the concurrent transmission/reception capability. The performance limit of full-duplex and its dominating factors are yet to be investigated.

Since the landmark paper of Gupta and Kumar [6], substantial effort has focused on analyzing wireless network capacity under various topologies and PHY layer technologies [24]. Existing analysis mostly assumes half-duplex radios, and targets capacity scaling laws under an asymptotically growing node population. Information theoretic properties of single-cell full-duplex WLAN are analyzed recently [25]. Yet it remains an open problem what is the fundamental gain when full-duplex interplays with multi-cell interference and spatial reuse.

Recent work of Yang *et al.* [26] used a simplified unit-disk model to compare the asymptotic dominance relation (higher or lower) between MIMO and full-duplex radio modes. Xie and Zhang [10] are the first to derive an upperbound of full-duplex network capacity through disk-packing. In contrast, our approach leverages stochastic geometry for an *average-*

case analysis of the full-duplex capacity and its gain over half-duplex. Our analysis shows consistent trend with [10], *i.e.*, the gain decreases as link distance approaches interference range. However, our framework can analyze the impact of a more comprehensive set of network parameters, carrier sensing models, and interference model. Our analysis also explains why the practical gain of full-duplex can exceed the upperbound in [10] that does not consider carrier sensing artifacts (caused by hidden/exposed terminals).

More recently, Tong and Haenggi [27] analyzed throughput of ALOHA for full-duplex and half-duplex hybrid network. Atzeni and Kountouris [28] analyze full-duplex MIMO, and also testifies full-duplex gain of less than 2 for realistic scenarios. Mohammadi *et al.* [29] analyze networks with full-duplex APs supporting simultaneous downlink and uplink, and show that even with imperfect self-interference cancellation, full-duplex network can still outperform half-duplex. Wang *et al.* [30] reveal severe aggregate interference affects full-duplex capacity gain, and prove that self-interference cancellation alone is not enough to scalable full duplex gain. In [31], Qin *et al.* consider end-to-end throughput in multi-hop wireless networks, and show that full-duplex can achieve throughput gain of more than 2 under oracle centralized scheduling. All above-mentioned work focus on ALOHA networks, but our work consider the more practical cases for CSMA networks, which is non-trivial especially consider the sophisticated models for imperfect carrier sensing and RTS/CTS.

Stochastic geometry has shown great potential in quantifying the spatial reuse in wireless networks [7]. Particularly to IEEE 802.11 networks, the key analytic question lies in approximating the *sparsified* winning node distribution after contention [15]. In [8], an HCPP model is proposed to capture key properties of 802.11 networks (for Poisson node distribution). Alfano *et al.* [32] extended model to analyze the nodes' throughput variation under a minimum link-distance constraint. Substantial work has focused on more accurate approximation of contention behavior [15]. Our recent analytical framework in [33] represents the first to advance stochastic geometry to analyze full-duplex wireless networks. Our analysis overcomes the limitations of classical stochastic geometry (Sec. II), and enables an investigation of different carrier sensing schemes for both full- and half-duplex networks. In the present work, we further enrich [33] with detailed models/proofs for the full-duplex gain under protocol/physical models, and for the asymptotic comparison of the two full-duplex modes (bi-directional transmission vs. cut-through transmission). We also establish a set of new analysis for ALOHA networks, which consolidates the important tradeoff between doubling link capacity and worsening spatial (interference) footprint.

VI. Conclusion

We have devised a stochastic geometry framework to analyze the spatial footprint of full-duplex and half-duplex links under perfect/imperfect carrier sensing and RTS/CTS signaling. Our framework introduces a new analytic tool, *i.e.*, the mean contention region, that integrates classical stochastic geometry with the protocol interference model. This allows us to establish closed-form formulas for the full-duplex gain under different topological properties and protocol imperfectness. Our analysis shows that, if carrier sensing is perfect, then the full-duplex gain approaches 2 only when inter-link interference is negligible (link distance approaches 0 and network density approaches 1). A broader implication is that the full-duplex gain diminishes a lot in centrally scheduled networks (no carrier sensing artifact) and multi-hop networks (link distance needs to be long to satisfy asymptotic connectivity constraint). In addition, if the hardware cost is the same, then MIMO is always better than full-duplex as it increases link capacity without adding extra interference footprints.

Appendix

A. Parameters in Theorem 3

The intermediate parameters in Theorem 3 are given by:

$$\gamma_1 = \arccos(\frac{R_I^2 + d^2 - {R_S}^2}{2dR_I}) \quad \gamma_2 = \arccos(\frac{{R_S}^2 + d^2 - R_I^2}{2dR_S})$$

$$\theta_1 = \arccos(\frac{d^2 + r^2 - R_I^2}{2dr}) \quad \theta_2 = \arccos(\frac{r^2 + R_I^2 - d^2}{2rR_I})$$

$$\theta_3 = \arccos(\frac{r^2 + {R_S}^2 - d^2}{2rR_S}) \quad \theta_4 = \arccos(\frac{d^2 + r^2 - {R_S}^2}{2dr}$$

$$\theta_5 = \arccos(\frac{r}{2R_S}) \quad \theta_6 = \arccos(\frac{r}{2R_I})$$

$$\varphi_1 = \arccos(\frac{{\delta_1}^2 + d^2 - R_I^2}{2d\Delta_1}), \quad \varphi_2 = \arccos(\frac{{\delta_1}^2 + {\delta_2}^2 - d^2}{2\delta_1\delta_2})$$

$$\varphi_3 = \arccos(\frac{{\delta_2}^2 + d^2 - {R_S}^2}{2d\delta_2}),$$

$$\varphi_4 = \arccos(\frac{2r^2 + 2dr\cos(\theta)}{2r\sqrt{d^2 + r^2 + 2dr\cos(\theta)}})$$

$$\varphi_5 = \arccos(\frac{2d^2 + r^2 + 2dr\cos(\theta) - R_I^2}{2d\sqrt{d^2 + r^2 + 2dr\cos(\theta)}})$$

$$\delta_1 = \sqrt{r^2 + R_I^2 + 2rR_I\cos(\theta - \gamma_1)}$$

$$\delta_2 = \sqrt{r^2 + {R_S}^2 - 2rR_S\cos(\theta + \gamma_2)}$$

B. Parameters and Proof for Theorem 4

The intermediate parameters in Theorem 4 are given by:

$$\theta_1 = \arccos(\frac{d^2 + r^2 - R_I^2}{2dr}) \quad \theta_2 = \arccos(\frac{r^2 + R_I^2 - d^2}{2rR_I})$$

$$\theta_3 = \arccos(\frac{d}{2R_I}) \quad \theta_4 = \arccos(\frac{r}{2R_I})$$

$$\theta_5 = \arccos(\frac{2R_I^2 - d^2}{2R_I^2})$$

$$\varphi_1 = \arccos(\frac{{\delta_1}^2 + d^2 - R_I^2}{2d\delta_1}),$$

$$\varphi_2 = \arccos(\frac{{\delta_1}^2 + {\delta_2}^2 - d^2}{2\delta_1\delta_2})$$

$$\varphi_3 = \arccos(\frac{{\delta_2}^2 + d^2 - R_I^2}{2d\delta_2})$$

$$\delta_1 = \sqrt{r^2 + R_I^2 + 2rR_I\cos(\theta - \theta_3)}$$

$$\delta_2 = \sqrt{r^2 + R_I^2 - 2rR_I\cos(\theta + \theta_3)}$$

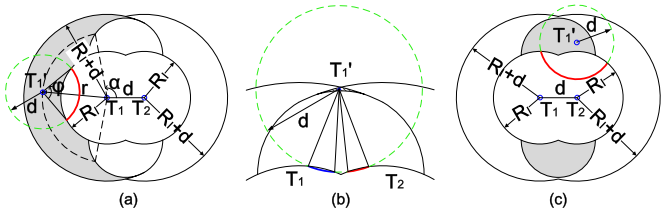

Fig. 16. (a) The left-hand side area in second situation, (b) the overlaying area of left-hand side area and right-hand side area, (c) the area in third situation.

Proof: We consider three regions shown as different patterns in Fig. 4(c) around typical link $\mathcal{L}_o$.

First, the union of primary transmitter T_1's and secondary transmitter T_2's interference range (V_1), should be counted as a deterministic contention region.

Second, consider a contending link $\mathcal{L}'$ whose primary transmitter $T_1^{'}$ exists within the grey area in Fig. 16(a), then its associated secondary transmitter $T_2^{'}$ may be located within T_1's interference range, which leads to contention with $\mathcal{L}_o$. The derivation of this spatial averaged contention region (V_2) is similar to Theorem 1. The symmetric region on the RHS in the same figure can be calculated in the same way.

There is a small area (shaded area in Fig. 16(b)) that needs special consideration: if another primary transmitter $T_1^{'}$ resides there, its secondary transmitter $T_2^{'}$ could fall in T_1 or T_2's interference range. For the LHS, we only need to consider $T_2^{'}$ is located within T_1's interference range; and similarly RHS for T_2's interference range.

Third, consider a contending link $\mathcal{L}'$ with its transmitter lying in the upper shaded area in Fig. 16(c). The associated secondary transmitter $T_2^{'}$ can reside in both primary transmitter T_1 and secondary transmitter T_2's interference range. This is different from situation 2 as the potential location of $T_2^{'}$ is continuous, which corresponds to V_3.

Finally, any area outside the above cases falls outside the potential contention region of the typical full-duplex link. □

C. Proof of Theorem 9

Proof: We first introduce the following definitions, considering the two full-duplex pairs q_i and q_j shown in Fig. 17.

(a) B_1 to be the set of (r,θ,ϕ,δ) values such that X_j and X_i are within R_C of each other. We similarly define B_2, B_3, B_4 for the cases when X_j and Y_i are within R_C of each other, Y_j and X_i are within R_C of each other, and Y_j and Y_i are within R_C of each other, respectively. Thus we have,

$$\begin{aligned}
B_1 &= \{(r,\theta,\phi,\delta) : r \le R_C\},\\
B_2 &= \{(r,\theta,\phi,\delta) : r^2 + d^2 - 2rd\cos(\theta-\phi) \le R_C^2\},\\
B_3 &= \{(r,\theta,\phi,\delta) : r^2 + d^2 + 2rd\cos(\theta-\delta) \le R_C^2\},\\
B_4 &= \{(r,\theta,\phi,\delta) : [(r\cos\theta + d\cos\delta) - d\cos\phi]^2\\
&\quad + [(r\sin\theta + d\sin\delta) - d\sin\phi]^2 \le R_C^2\}
\end{aligned}$$

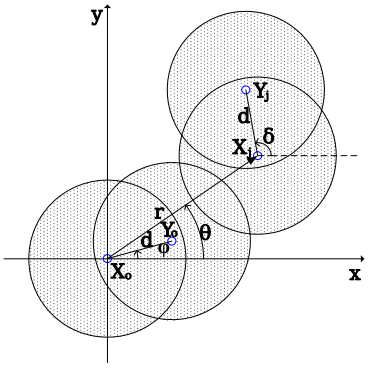

Fig. 17. Illustration of two full-duplex pairs.

(b) $V_1(r,\theta,\phi,\delta)$ is the mean contention region around two pairs q_i and q_j that are contending with other full-duplex links.

$$\begin{aligned}
&\Delta(r,\theta,\phi,\delta)\\
&= \ln\Big(1 + \frac{\beta}{2}d^{\alpha}\Big\{r^{-\alpha} + \big(r^2 + d^2 + 2rd\cos(\theta-\delta)\big)^{-\frac{\alpha}{2}}\\
&\quad + \big(r^2 + d^2 - 2rd\cos(\theta-\phi)\big)^{-\frac{\alpha}{2}} + (\,[(r\cos\theta + d\cos\delta)\\
&\quad - d\cos\phi]^2 + [(r\sin\theta + d\sin\delta) - d\sin\phi]^2\,)^{-\frac{\alpha}{2}}\Big\}\Big)
\end{aligned}$$

The probability that two nodes in a pair successfully transmit to each other, $\mathbb{P}^{!o}_{\Phi_m^F}(SIR_{X_o} > \beta, SIR_{Y_o} > \beta)$ can be upper bounded by,

$$\begin{aligned}
&\mathbb{P}^{!o}_{\Phi_m^F}\Big(h_o > \frac{\beta}{2}d^{\alpha}\sum_{q_j\in\Phi_m^F} h_j^o\{\,\|X_j - X_o\|^{-\alpha} + \|Y_j - X_o\|^{-\alpha}\\
&\qquad + \|X_j - Y_o\|^{-\alpha} + \|Y_j - Y_o\|^{-\alpha}\,\}\Big) \qquad (40)
\end{aligned}$$

Later in the proof, we get a lower bound on (40) using *Jensen's* inequality which serves as an estimate of $\mathbb{P}^{!o}_{\Phi_m^F}(SIR_{X_o} > \beta, SIR_{Y_o} > \beta)$. We validate this estimate by comparing it to the simulation results. We first obtain (40) by conditioning it the orientation ϕ of the secondary transmitter of the typical pair. To reduce notational complexity, we will denote this conditioning in the Reduced Palm measure as $\mathbb{P}^{!o,\phi}_{\Phi_m^F}$. Then, in the end we obtain the estimate by deconditioning *w.r.t* ϕ. Also, in the following lines of the proof we will denote the term $\{\|X_j - X_o\|^{-\alpha} + \|Y_j - X_o\|^{-\alpha} + \|X_j - Y_o\|^{-\alpha} + \|Y_j - Y_o\|^{-\alpha}\}$ in (40) by l_j^o. Thus we have,

$$\begin{aligned}
&\mathbb{P}^{!o,\phi}_{\Phi_m^F}\Big(h_o > \frac{\beta}{2}d^{\alpha}\sum_{q_j\in\Phi_m^F} h_j^o l_j^o\Big)\\
&= \mathbb{E}^{!o,\phi}_{\Phi_m^F,h_j^o}\left[exp\left\{-\frac{\beta}{2}d^{\alpha}\sum_{q_j\in\Phi_m^F} h_j^o l_j^o\right\}\right] \qquad (41)\\
&= \mathbb{E}^{!o,\phi}_{\Phi_m^F}\left[\prod_{q_j\in\Phi_m^F}\mathbb{E}_{h_j^o}\left[exp\left\{-\frac{\beta}{2}d^{\alpha}h_j^o l_j^o\right\}\right]\right] \qquad (42)\\
&= \mathbb{E}^{!o,\phi}_{\Phi_m^F}\left[exp\left\{-\sum_{q_j\in\Phi_m^F}\ln\left(1 + \frac{\beta}{2}d^{\alpha}l_j^o\right)\right\}\right]
\end{aligned}$$

$$> exp\left\{-\mathbb{E}^{!o,\phi}_{\Phi^F_m}\left[\sum_{q_j\in\Phi^F_m}\ln\left(1+\frac{\beta}{2}d^{\alpha}l^o_j\right)\right]\right\} \tag{43}$$

$$= exp\left\{-\mathbb{E}^{!o,\phi}_{\Phi^F_m}\left[\sum_{q_j\in\Phi^F_m}\ln\left(1+\frac{\beta}{2}d^{\alpha}\left(\|X_j-X_o\|^{-\alpha}\right.\right.\right.\right.$$
$$\left.\left.\left.\left.+\ \|Y_j-X_o\|^{-\alpha}+\|X_j-Y_o\|^{-\alpha}+\|Y_j-Y_o\|^{-\alpha}\right)\right)\right]\right\} \tag{44}$$

$$= exp\left\{-\mathbb{E}^{!o,\phi}_{\Phi^F_m}\left[\sum_{(r,\theta,\delta)\in\Phi^F_m}\Delta(r,\theta,\phi,\delta)\right]\right\}$$
$$= exp\left\{-\frac{1}{\lambda^f_m}\int_0^{\infty}\int_0^{2\pi}\int_0^{2\pi}\rho^{(2)}(r,\theta,\phi,\delta)\Delta(r,\theta,\phi,\delta)r\mathrm{d}r\mathrm{d}\theta\mathrm{d}\delta\right\} \tag{45}$$

$$= exp\left\{-\frac{\lambda^2_p}{2\pi\lambda^f_m}\int_0^{\infty}\int_0^{2\pi}\int_0^{2\pi}k(r,\theta,\phi,\delta)\Delta(r,\theta,\phi,\delta)r\mathrm{d}r\mathrm{d}\theta\mathrm{d}\delta\right\} \tag{46}$$

To derive Eq. (41), we condition on the point process Φ^F_m and h^o_j and use the fact that h_o is an exponential random variable with $\mathbb{E}(h_o)=1$. As $\{h^o_j\}$ are a set of *i.i.d* random variables, Eq. (42) follows straightforwardly. To get Eq. (43), we apply *Jensen's* inequality using the fact that $exp(-.)$ is a strictly convex function. We get Eq. (44) by simply replacing l^o_j with the terms in Eq. (40) mentioned previously. Eq. (45) is obtained by applying *Campbell's* theorem [17] to the previous step. To get Eq. (46), we use the relation between *second-order product density* of the stationary point process Φ^F_m and $k(r,\theta,\phi,\delta)$ based on [21]. Finally, by deconditioning Eq. (46) *w.r.t* ϕ, we get a lower bound on (40) which is the estimation in Theorem 9 . We note that the function $g(V_1)$ can be obtained in an analogous manner to the derivation of the function $\eta(V)$ given the analysis of mean interference for *Matèrn* type II process in *Zhong et al.* [9]. □

REFERENCES

[1] Kumu Networks. (2014). *Wireless Full-duplex: A Revolution in Wireless Design*. [Online]. Available: http://kumunetworks.com/

[2] J. I. Choi, M. Jain, K. Srinivasan, P. Levis, and S. Katti, "Achieving single channel, full duplex wireless communication," in *Proc. ACM MobiCom*, 2010, pp. 1–12.

[3] D. Bharadia, E. McMilin, and S. Katti, "Full duplex radios," in *Proc. ACM SIGCOMM*, 2013, pp. 375–386.

[4] W. Zhou, K. Srinivasan, and P. Sinha, "RCTC: Rapid concurrent transmission coordination in full duplex wireless networks," in *Proc. IEEE ICNP*, Oct. 2013, pp. 1–10.

[5] A. Sahai, G. Patel, and A. Sabharwal, "Pushing the limits of full-duplex: Design and real-time implementation," *CoRR*, vol. abs/1107.0607, Dec. 2011.

[6] P. Gupta and P. Kumar, "The capacity of wireless networks," *IEEE Trans. Inf. Theory*, vol. 46, no. 2, pp. 388–404, Mar. 2000.

[7] J. G. Andrews, R. K. Ganti, M. Haenggi, N. Jindal, and S. Weber, "A primer on spatial modeling and analysis in wireless networks," *IEEE Commun. Mag.*, vol. 48, no. 11, pp. 156–163, Nov. 2010.

[8] H. Q. Nguyen, F. Baccelli, and D. Kofman, "A stochastic geometry analysis of dense IEEE 802.11 networks," in *Proc. IEEE INFOCOM*, May 2007, pp. 1199–1207.

[9] Y. Zhong, W. Zhang, and M. Haenggi, "Stochastic analysis of the mean interference for the RTS/CTS mechanism," in *Proc. IEEE ICC*, Jun. 2014, pp. 1996–2001.

[10] X. Xie and X. Zhang, "Does full-duplex double the capacity of wireless networks?" in *Proc. IEEE INFOCOM*, Apr./May 2014, pp. 253–261.

[11] F. Baccelli, B. Blaszczyszyn, and P. Muhlethaler, "Stochastic analysis of spatial and opportunistic aloha," *IEEE J. Sel. Areas Commun.*, vol. 27, no. 7, pp. 1105–1119, Sep. 2009.

[12] S. Gollakota and D. Katabi, "Zigzag decoding: Combating hidden terminals in wireless networks," in *Proc. ACM SIGCOMM*, 2008, pp. 159–170.

[13] M. Vutukuru, K. Jamieson, and H. Balakrishnan, "Harnessing exposed terminals in wireless networks," in *Proc. USENIX NSDI*, 2008, pp. 59–72.

[14] X. Xie and X. Zhang, "Semi-synchronous channel access for full-duplex wireless networks," in *Proc. IEEE ICNP*, Oct. 2014, pp. 209–214.

[15] A. Busson and G. Chelius, "Point processes for interference modeling in CSMA/CA ad-hoc networks," in *Proc. ACM PE-WASUN*, 2009, pp. 33–40.

[16] M. Haenggi, *Stochastic Geometry for Wireless Networks*. Cambridge, U.K.: Cambridge Univ. Press, 2013.

[17] A. M. Ibrahim, T. A. ElBatt, and A. El-Keyi, "Coverage probability analysis for wireless networks using repulsive point processes," *CoRR*, vol. abs/1309.3597, Oct. 2013.

[18] B. Matérn, *Spatial Variation* (Lecture Notes in Statistics), vol. 36. New York, NY, USA: Springer, 1986.

[19] M. Haenggi, "Mean interference in hard-core wireless networks," *IEEE Commun. Lett.*, vol. 15, no. 8, pp. 792–794, Aug. 2011.

[20] M. Haenggi and R. K. Ganti, "Interference in large wireless networks," *Found. Trends Netw.*, vol. 3, no. 2, pp. 127–248, Feb. 2008.

[21] D. Stoyan and H. Stoyan, "On one of Matérn's hard-core point process models," *Math. Nachrichten*, vol. 122, no. 1, pp. 205–214, 1985.

[22] F. Baccelli and B. Blaszczyszyn, *Stochastic Geometry and Wireless Networks: Theory*, vol. 1. Breda, The Netherlands: Now, 2010.

[23] M. Haenggi and R. K. Ganti, "Interference in large wireless networks," *Found. Trends Netw.*, vol. 3, no. 2, pp. 127–248, 2009. [Online]. Available: http://dx.doi.org/10.1561/1300000015

[24] C. Jiang *et al.*, "Toward simple criteria to establish capacity scaling laws for wireless networks," in *Proc. IEEE INFOCOM*, Mar. 2012, pp. 774–782.

[25] V. Aggarwal, M. Duarte, A. Sabharwal, and N. K. Shankaranarayanan, "Full- or half-duplex? A capacity analysis with bounded radio resources," in *Proc. IEEE Inf. Theory Workshop (ITW)*, Sep. 2012, pp. 207–211.

[26] Y. Yang, B. Chen, K. Srinivasany, and N. B. Shroff, "Characterizing the achievable throughput in wireless networks with two active RF chains," in *Proc. IEEE INFOCOM*, Apr./May 2014, pp. 262–270.

[27] Z. Tong and M. Haenggi, "Throughput analysis for full-duplex wireless networks with imperfect self-interference cancellation," *IEEE Trans. Commun.*, vol. 63, no. 11, pp. 4490–4500, Nov. 2015.

[28] I. Atzeni and M. Kountouris, "Full-duplex MIMO small-cell networks: Performance analysis," in *Proc. IEEE GLOBECOM*, Dec. 2015, pp. 1–6.

[29] M. Mohammadi, H. A. Suraweera, Y. Cao, I. Krikidis, and C. Tellambura, "Full-duplex radio for uplink/downlink wireless access with spatially random nodes," *IEEE Trans. Commun.*, vol. 63, no. 12, pp. 5250–5266, Dec. 2015.

[30] X. Wang, H. Huang, and T. Hwang, "On the capacity gain from full duplex communications in a large scale wireless network," *IEEE Trans. Mobile Comput.*, vol. 15, no. 9, pp. 2290–2303, Sep. 2015.

[31] X. Qin *et al.*, "Impact of full duplex scheduling on end-to-end throughput in multi-hop wireless networks," *IEEE Trans. Mobile Comput.*, vol. 16, no. 1, pp. 158–171, Jan. 2017.

[32] G. Alfano, M. Garetto, and E. Leonardi, "New insights into the stochastic geometry analysis of dense CSMA networks," in *Proc. IEEE INFOCOM*, Apr. 2011, pp. 2642–2650.

[33] S. Wang, V. Venkateswaran, and X. Zhang, "Exploring full-duplex gains in multi-cell wireless networks: A spatial stochastic framework," in *Proc. IEEE INFOCOM*, Apr./May 2015, pp. 855–863.

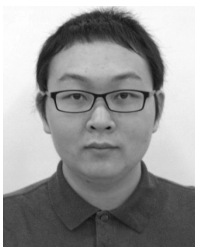

Shu Wang received the B.E. degree from the Harbin Institute of Technology, China, in 2013, and the M.S. degree from the University of Wisconsin-Madison in 2015. He is currently pursuing the Ph.D. degree with the Department of Computer Science, The University of Chicago. His research interests include distributed system, system reliability, and networking.

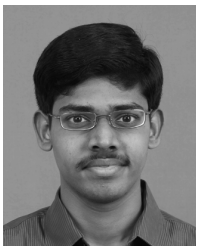

Vignesh Venkateswaran received the B.Tech. degree in electrical engineering from the Indian Institute of Technology (IIT) Mandi, Suran, India, and the M.S. degree in electrical engineering from the University of Wisconsin-Madison, Madison, WI, USA. He is currently a Software Engineer with the Data Center Networking, Cisco Systems Inc., San Jose, CA, USA. His research interests include system software development for network analytics on next-generation data center networking switches.

Xinyu Zhang received the Ph.D. degree in computer science and engineering from the University of Michigan in 2012. He is currently an Assistant Professor with the Department of Electrical and Computer Engineering, University of Wisconsin-Madison. His research interest lies in wireless sensing algorithms that facilitate the Internet-of-Things applications and radical architectures for next-generation wireless networks, based on millimeter-wave and large-scale MIMO. He received the ACM MobiCom Best Paper Award in 2011 and the NSF CAREER award in 2014.